# Terminal Loop Sequences in Viral Double-Stranded RNAs Modulate RIG-I Signaling

Matthew Hackbart[1], Patrick Wang[1], Victoria Gnazzo[1], and Carolina B. López[1,2*]

[1]Department of Molecular Microbiology, Washington University School of Medicine, St. MO

[2]Center for Women Infectious Disease Research, Washington University School of Medicine, St. MO

[*]Corresponding Author, clopezzalaquett@wustl.edu

## ABSTRACT

Detection of foreign RNAs is a crucial activation step for innate immunity pathways in response to viral infections. Retinoic acid-inducible gene I (RIG-I) is a cytoplasmic RNA sensor that triggers type I and III interferon (IFN) expression and activates the antiviral response. The activating ligand for RIG-I has been shown to be 5'-triphosphated blunt-ended double stranded(ds) RNA, but questions remain on the molecular mechanisms for RIG-I activation during viral infections. Here we show that immune-activating copy-back viral genomes (cbVGs) contain RNA stem loops away from the 5' end of the RNA that enhance RIG-I signaling and IFN expression. Importantly, the sequence of the terminal loops of the activating motifs impacts the strength of IFN expression. Additionally, we show that synthetic versions of these cbVG-derived stem loops trigger innate immune responses in mice demonstrating their potential as immunostimulants *in vivo*.

## INTRODUCTION

Retinoic acid-inducible gene I (RIG-I) is an important cytoplasmic sensor of viral infections that initiate the antiviral immune response. The RIG-I-like receptor (RLR) family includes RIG-I, melanoma differentiation-associated protein 5 (MDA5), and laboratory of genetics and physiology 2 (LGP2), which are host proteins that bind to RNAs and initiate the antiviral response[1,2]. Binding of RLRs by foreign RNA triggers a signaling cascade through the mitochondrial antiviral signaling (MAVS) protein that ends in the expression of antiviral proteins, including type I and III interferons (IFNs)[3-7]. RIG-I contains a C-terminal regulatory domain that recognizes the foreign RNA and drives conformational changes in the protein helicase domain to wrap around the RNA[8-13]. These conformational changes also release caspase activation and recruitment domains (CARDs) that promote oligomerization of the RIG-I proteins and signaling through MAVS[3,14,15]. RLRs recognize unique pathogen associated molecular patterns (PAMPs) found in foreign RNA but not in the host cell RNAs.

The most well-studied of the RLR PAMPs are within the RNAs that activate RIG-I. The regulatory domain of RIG-I detects terminal 5' triphosphates on RNA[16-19] and the detection of this motif can be inhibited by methylation of the 5' end of the RNA[20,21]. While ssRNA can activate RIG-I, the highest activation occurs when blunt ended dsRNA[22] contains the 5' triphosphate[17]. The addition of overhangs to the end of the dsRNA limits activation of RIG-I[18,19]. RIG-I is activated best by short dsRNA while longer synthetic dsRNAs such as poly I:C (> 500nt in length) activate MDA5[23-25]. With these guidelines in place, minimal ligands for activating RIG-I that contain a short 10 base pair dsRNA stem with a 5' triphosphate have been synthetically generated[26,27]. While these studies have provided critical data to identify the motifs that RIG-I will bind to in the RNA, in general,

48 they are not based on RNAs found naturally during viral infections. Further work is thus
49 needed to confirm and identify the characteristics of viral RNAs that activate RIG-I
50 signaling during infection.

51 Previously, we and others determined that the RNA that most robustly activates
52 RIG-I signaling during Sendai Virus (SeV) infection is a copy-back viral genome (cbVG)[28-
53 30]. CbVGs contain complementary ends predicted to form a blunt-ended dsRNA PAMP
54 with a 5' triphosphate, characteristic of the canonical RIG-I ligand[31,32]. However, detailed
55 folding analyses of the most prominent cbVG from SeV (cbVG 546) revealed a much
56 more complex folding of the molecule, including a stem loop that is necessary for strong
57 activation of the RIG-I pathway to stimulate IFN expression. This stem loop is comprised
58 of nucleotides 70-114 of cbVG 546, and when transferred to inert RNAs, it significantly
59 enhanced the immunostimulatory capability of the RNA[33]. Interestingly, the removal of
60 stem loop 70-114 from cbVG 546 severely decreased RIG-I activation even though the
61 cbVG still contained the 5' triphosphate and blunt-end dsRNA.

62 It is unknown how SeV 70-114 enhanced RIG-I activity or whether other RIG-I
63 stimulatory cbVGs contain stem loops similar to SeV 70-114. We therefore sought to
64 determine if other viral cbVGs contain RNA stem loops that can transfer RIG-I stimulatory
65 activity to otherwise inert RNAs and identify features of these RNA stem loops that are
66 necessary for robust RIG-I activation. Here, we identified multiple sequences in cbVGs
67 from human respiratory syncytial virus (RSV) and Nipah virus (NiV) infections that can
68 transfer RIG-I stimulatory activity to the inert X RNA from the hepatitis C virus. Through
69 mutation of the terminal loop sequences of the cbVG-derived RNAs, we discovered that
70 specific nucleotides in the terminal loop of the RNA are necessary for strong activation of

71 RIG-I signaling in cells. Lastly, *in vivo* administration of the cbVG-derived RNA loops
72 activated innate immune signaling pathways, suggesting their potential use as
73 immunostimulants for vaccines and immunotherapies.
74
75 **RESULTS**
76 **RSV and NiV cbVGs stimulate interferon expression**
77 To identify additional natural RNA stem loops that could activate antiviral innate
78 immune pathways, we selected previously identified cbVGs from either RSV (RSV cbVG
79 236)[34] and NiV (DI15, here called NiV cbVG 378)[35]. We first determined if these cbVGs
80 can activate the IFN signaling pathway in human A549 lung cells and found that *in vitro*
81 transcribed RNAs of both RSV cbVG 236 and NiV cbVG 378 could stimulate the
82 transcription of type I (*IFNB1*) and type III (*IFNL1)* interferons at 6 hours post transfection,
83 but not the hepatitis C virus X region (Fig 1A and 1B). This IFN activation was largely
84 MAVS-dependent, confirming activation of the RLR signaling, similar to what we had
85 reported for SeV cbVG 268, a shortened version of cbVG 546 (Fig 1C)[33].
86
87 **RSV cbVGs contain immunostimulatory stem loops**
88 To identify which specific RSV cbVG 236 sequence confers a strong RIG-I
89 stimulatory activity to the molecule, we first made a series of deletions in cbVG 236 that
90 either removed internal sequences disrupting the stem loops or removed a
91 complementary end of the cbVG (Fig 2A). We found that nucleotides 1-48 and 189-236
92 in the complementary ends of cbVG 236 contribute to RIG-I activation, as deletion
93 mutants del 1-48 and 189-236 lost immunostimulatory activity (Fig 2B). Interestingly, we

94 also found that nucleotides 49-100 are necessary for maximum IFN expression. Mutants
95 with deletions in this range (del 49-187 and del 64-187) show reduced stimulation of the
96 IFN response, but del 101-147 and del 137-187 induced strong IFN expression.

97 To determine if these RNA sequences can enhance expression of IFNs to an
98 otherwise inert RNA molecule, we transferred the RSV cbVG sequences to the inert X
99 RNA motif from the hepatitis C virus, ensuring that the overall structures of the final
100 molecules were similar (Fig S2)[36]. We found that X-region chimeras carrying RSV cbVG
101 sequences 1-48 or 39-68 induced the highest IFN expression when transfected into A549
102 cells, but RSV cbVG sequence 189-236 did not significantly enhance IFN expression in
103 this context (Fig 2C), suggesting that additional features of the 189-236 region participate
104 in inducing IFN expression.

105 To determine if specific immunostimulatory stem loops were present within the
106 immunostimulatory sequences, we then performed *in silico* prediction of the RNA stem
107 loops using RNAfold[37]. Since the complement ends of the cbVGs interfere with the *in*
108 *silico* folding predictions based on minimal free energy, and it is likely that favorable
109 secondary structures form during RNA synthesis rather than once the entire molecule has
110 been produced, we determined all possible RNA structures on partial cbVGs lacking
111 either the 3' or 5' complementary sequences. RSV cbVG 236 was predicted to form five
112 RNA stem loops (Fig 2D and Fig S1) in the absence of 3'-5' complementation with two of
113 the stem loops (1-34 and 39-68) present within the immunostimulatory sequences. RNA
114 folding of X region + RSV 1-48 predicted an immunostimulatory stem loop of sequence
115 1-34 similar to the full length cbVG (Fig S2).

116

117 **NiV cbVGs contain immunostimulatory stem loops**

118 Similar to RSV, we made a series of deletions to remove specific RNA sequences
119 from NiV cbVG 378 and determined which portions of the cbVG are necessary for strong
120 IFN expression. We found that nucleotides within the complementary ends of the cbVG
121 were necessary for strong expression of IFNs and removal of nucleotides 325-360 also
122 decreased IFN expression (Fig 3A and B). When attached to the X RNA, we found that
123 while NiV 325-360 induced *IFNB1* and *IFNL1* expression, NiV sequences 44-78 and 85-
124 136 induced greater IFN expression (Fig 3C). NiV cbVG 378 is predicted to have eight
125 RNA stem loops (Fig 3D and Fig S3) with stem loops of NiV 44-78 and NiV 85-136
126 enhancing IFN stimulation when transferred to the inert X RNA. Unexpectedly, deletion
127 of 44-78 or 85-136 sequences did not significantly reduce *IFNL1* expression from upon
128 RNA transfection, suggesting that the RNA folds differently in these regions of the
129 complementary ends than what was predicted *in silico*.

130

131 **Terminal loop sequences are critical for IFN expression**

132 We next investigated the characteristics conserved among high
133 immunostimulatory RNA sequences versus lower immunostimulatory sequences (Fig
134 4A). The cbVG RNAs are predicted to form stem loops that are diverse in their size and
135 shape. However, two complementary sequences that are predicted to form loops with the
136 same structure (RSV 1-34 and RSV 203-236) exhibit different immunostimulatory
137 capabilities (Fig 2C). We did not observe significant differences in the minimum free
138 energy (MFE) between the stem loops, most of which had a predicted MFE between -6
139 and -10 kcal/mol. Upon observation, we found that the terminal loops with the higher

140 immunostimulatory activity contain either a CAA motif or poly-A stretch at the tip of the
141 loop (Fig 4A). In contrast, the low immunostimulatory loops are instead U-rich at the
142 terminal loop residues, except for NiV 324-361 which contains an A-rich terminal loop.

143 We then hypothesized that the terminal loop adenines played a key role in
144 triggering RIG-I signaling. To test this hypothesis, we mutated the terminal loops of the
145 X-RNA attached sequences and tested their ability to induce IFN expression. Mutation of
146 the terminal loop sequence did not alter the overall structure of the stem loops (Fig S4-
147 7). For X + SeV 70-114, we found that mutation of the A89 or A90 terminal residues
148 greatly reduced IFN activation by the RNA construct, however mutation of the C88
149 residue did not (Fig 4B). Mutations in X + RSV 1-48 showed that A18, but not C17 or A19,
150 was necessary for full IFN activation (Fig 4C). Additionally, mutation of X + NiV 85-136
151 showed that both terminal adenines, A111 and A112, were necessary for IFN signaling
152 (Fig 4D). However, this trend was not observed for the low immunostimulatory X + NiV
153 324-361, which did not show a reduction in IFN stimulation upon mutation of the terminal
154 adenines (Fig 3E). These data suggest that terminal adenines are critical to trigger robust
155 IFN expression and that additional sequence-specific factors impact their stimulatory
156 activity.

157

158 **RSV 1-48 activates innate immune signaling *in vivo***

159 Previously, we found that the SeV cbVG 546 stem loop 70-114 activates a strong
160 type I immune responses in mice when administered alone or within a lipid nanoparticle
161 (LNP)[38-40]. Here, we aimed to determine whether RSV sequence 1-48 similarly activates
162 innate sensors and induces an immune response *in vivo*. To ensure the RNA constructs

163 were delivered intracellularly to trigger the RIG-I pathway, we packaged the X + RSV 1-
164 48 and the control X + RSV 189-236 chimera constructs into LNPs (Fig 5A) and confirmed
165 the homogeneity of the formulations before *in vivo* administration (Fig 5B). These
166 formulations were then administered subcutaneously in the footpad of C57BL/6 mice.
167 After 16 hours, we found that LNPs containing X + RSV 1-48 induced significantly higher
168 expression of *IFNB1*, *MX1*, *IL1B*, and *CXCL10* compared to empty LNPs and X + RSV
169 189-236 (Fig 5C). These data demonstrate that the RSV cbVG-derived 1-48 sequence
170 retains its immunostimulatory activity *in vivo* when packaged into LNPs and together with
171 data from SeV 70-114 demonstrate that small RNA motifs with terminal loop adenines
172 can serve as potent immunostimulators in mice.
173

174 **DISCUSSION**

175 We have identified multiple RNA stem loops derived from cbVGs of RSV and NiV
176 that can transfer robust IFN stimulatory capabilities to an inert RNA. One unique feature
177 of the higher immunostimulatory RNA stem loops is a richness for adenines at the tip of
178 the loop. When these sequences were mutated, the mutant RNAs stimulated significantly
179 less IFN upon transfection into cells. Upon packaging into lipid nanoparticles, the RSV
180 cbVG-derived stem loop was able to activate innate immune signaling in mice.

181 While the enhanced stimulation appears to occur with adenine-rich sequences, we
182 also observe that a stem loop with 5 adenines (NiV 325-360) did not have decreased IFN
183 activation when the adenines were mutated (Fig. 4E). Since an adenine-rich loop does
184 not always enhance IFN expression, more work is necessary to determine the exact motif
185 or motifs that make up an optimal terminal loop PAMP. Some possibilities are that

186 sequences in the stems of the RNA interact with the loop to alter binding or that host
187 proteins are recognizing a specific RNA motif that is more than adenines.

188 One major question that remains is what step of the RIG-I pathway is impacted by
189 these terminal adenine-rich sequence. We propose the following possibilities for how the
190 terminal loop sequences may alter IFN expression: 1) RIG-I is heavily modulated by
191 phosphorylation and ubiquitination by host proteins[41], so the terminal loop may recruit or
192 inhibit additional host factors from interacting and altering RIG-I function in cells. 2) MAVS
193 has recently been shown to interact with host RNAs[42]. The terminal sequence may
194 stabilize RIG-I binding to MAVS through RNA/MAVS interactions and enhance
195 downstream signaling to boost IFN expression. 3) The terminal loop adenines may be
196 prone to RNA modifications such as N6 methylation to generate N6 methyladenosine
197 (m6A)[43]. m6A RNA modification can alter the stability of the RNA in a cell and modulate
198 the binding of RNA binding proteins. 4) Other unknown host RNA-binding proteins support
199 robust RIG-I signaling. Further work is necessary to parse out what interactions occur
200 with this terminal loop sequence and why adenine-rich sequences enhance IFN
201 expression from the RIG-I pathway.

202 With the advent of mRNA vaccines and the usage of synthetic RNAs as
203 therapeutics, understanding how RNAs can activate innate immunity is crucial to
204 optimizing RNA-based adjuvants and treatments. Synthetic RNAs can act as immune
205 adjuvants during vaccination[27,38-40,44,45], and the addition of immunostimulatory stem
206 loops to mRNA vaccines may bypass the need for additional adjuvants such as alum.
207 Although additional work is necessary to assess the immunostimulatory properties of
208 RNA stem loops *in vivo*, our discovery that the terminal loop sequence modulates immune

209 activation can lead to the development of strategies to tailor the immune response not
210 only based on dosage of stimulatory RNA, but on the sequence of attached RNA stem
211 loops.
212
213 **MATERIALS AND METHODS**
214 **Cells and Reagents.** A549 human type II alveolar cells (ATCC, CCL-185) and MAVS-
215 KO A549 cells (gifted from S. Weiss) were cultured at 37°C and 5% $CO_2$ with Dulbecco's
216 modified Eagle's media (Thermofisher, 11995065) supplemented with 10% fetal bovine
217 serum (FBS), 1 mM sodium pyruvate, 2 mM L-Glutamine, and 50 mg/mL gentamicin. All
218 cell lines were treated with mycoplasma removal agent (MP Biomedicals, 093050044)
219 and routinely tested for mycoplasma before use.
220
221 ***In Vitro* Transcription of RNA.** RNAs were cloned into a pSL1180-T7 plasmid that
222 contains T7 promoter at the 5' end of the RNA sequence and hepatitis D virus ribozyme
223 after the RNA sequence. *In vitro* transcription was performed with the Megascript T7
224 Transcription Kit (Thermofisher, AM1334) and RNA was isolated with LiCl precipitation
225 according to manufacturer's protocols. Purified RNA was measured by Qubit and tested
226 for quality by Bioanalyzer (Agilent). Full protocol available Protocols.io:
227 dx.doi.org/10.17504/protocols.io.3byl49qprgo5/v2
228
229 **RT-PCR and qPCR.** A549 cells were transfected with 5 pmol of indicated RNA and
230 Lipofectamine 2000 (Thermofisher, 11668027). After 6 hours, RNA was isolated with
231 Trizol (Thermofisher, 15596026). cDNA was generated with random hexamers using the

232 High-Capacity RNA to cDNA kit (Thermofisher, 4387406) according to the manufacturer's
233 protocols. For qPCR quantification, cDNA was quantified with Power SYBR Green Mix
234 (Thermofisher, 4367660). *IFNL1, IFNB1, IL1B, MX1, and CXCL10* were normalized to a
235 house keeping index calculated from *ACTB* and *GAPDH* genes. Sequences of primers
236 are given in Table S1. Full protocol available at Protocols.io:
237 dx.doi.org/10.17504/protocols.io.8epv5rxw6g1b/v1
238

239 **Mice**

240 C57BL/6 mice (The Jackson Laboratory) were bred in house. All mice were sex
241 and age matched. Both male and female mice were included in the experiments.
242

243 **Lipid Nanoparticle formulation**

244 X + RSV 1-48 and X + RSV 189-236 were encapsulated in the GenVoy Ionizable
245 Lipid Mix (ILM) using a NanoAssemblr Ignite machine (Precision Nanosystems) following
246 the manufacturer's instructions. Empty LNPs were performed and used as controls.
247 Encapsulation efficiency and RNA concentration were tested by Ribogreen Assay
248 (ThermoFisher). Final particle size was measure by Dynamic Light Scattering. Full
249 protocol available at Protocols.io: dx.doi.org/10.17504/protocols.io.36wgqnn4kgk5/v1
250

251 **Mice immunization**

252 Mice were anesthetized with isoflurane and injected subcutaneously (s.c.) into a
253 rear footpad. For immune response studies mice were inoculated with 0.5 µg X 1-48; 0.5

254 μg X 189-236; Empty LNPs or PBS at a final volume of 30 μl per dose. RNA was extracted
255 from footpad 16 hours after inoculation using TRIzol (Ambion Inc.).
256
257 ***In Silico* RNA Folding Prediction.** All RNA folding predictions were performed using the
258 University of Vienna RNAfold website with the ViennaRNA Package (Version 2.6.3).
259 Structures shown are the minimum free energy structures. All sequences used for folding
260 are given in Table S2.
261 Website: http://rna.tbi.univie.ac.at/cgi-bin/RNAWebSuite/RNAfold.cgi
262
263 **Statistical Analysis and Reproducibility**
264 All statistics were calculated using GraphPad Prism. Version 9. Specific tests and
265 significance values are indicated in each figure legend. Data reported are biological
266 triplicates unless otherwise stated.
267
268 **Ethics statement**
269 All described studies adhered to the Guide for the Care and Use of Laboratory
270 Animal of the National Institute of Health. Institutional Animal Care and Use Committee,
271 Washington University in St. Louis approved protocol 23-0083.
272
273 **ACKNOWLEDGEMENTS**
274 The authors acknowledge the use of the Chemical and Environmental Analysis Facility at
275 Washington University in Saint Louis for instrumentation and analytical support.
276 **Funding:**
277 NIH T32 HL007317-44 (MH)

NIH T32 AI007163-45 (MH)

NIH A137062 (CBL)

WashU BJC Investigator Program (CBL)

## BIBLIOGRAPHY

1 Kato, H., Takahasi, K. & Fujita, T. RIG-I-like receptors: cytoplasmic sensors for non-self RNA. *Immunol Rev* **243**, 91-98 (2011). https://doi.org:10.1111/j.1600-065X.2011.01052.x

2 Thoresen, D. *et al.* The molecular mechanism of RIG-I activation and signaling. *Immunol Rev* **304**, 154-168 (2021). https://doi.org:10.1111/imr.13022

3 Yoneyama, M. *et al.* The RNA helicase RIG-I has an essential function in double-stranded RNA-induced innate antiviral responses. *Nat Immunol* **5**, 730-737 (2004). https://doi.org:10.1038/ni1087

4 Tanner, N. K. & Linder, P. DExD/H box RNA helicases: from generic motors to specific dissociation functions. *Mol Cell* **8**, 251-262 (2001). https://doi.org:10.1016/s1097-2765(01)00329-x

5 Kawai, T. *et al.* IPS-1, an adaptor triggering RIG-I- and Mda5-mediated type I interferon induction. *Nat Immunol* **6**, 981-988 (2005). https://doi.org:10.1038/ni1243

6 Seth, R. B., Sun, L., Ea, C. K. & Chen, Z. J. Identification and characterization of MAVS, a mitochondrial antiviral signaling protein that activates NF-kappaB and IRF 3. *Cell* **122**, 669-682 (2005). https://doi.org:10.1016/j.cell.2005.08.012

7 Xu, L. G. *et al.* VISA is an adapter protein required for virus-triggered IFN-beta signaling. *Mol Cell* **19**, 727-740 (2005). https://doi.org:10.1016/j.molcel.2005.08.014

8 Cui, S. *et al.* The C-terminal regulatory domain is the RNA 5'-triphosphate sensor of RIG-I. *Mol Cell* **29**, 169-179 (2008). https://doi.org:10.1016/j.molcel.2007.10.032

9 Kowalinski, E. *et al.* Structural basis for the activation of innate immune pattern-recognition receptor RIG-I by viral RNA. *Cell* **147**, 423-435 (2011). https://doi.org:10.1016/j.cell.2011.09.039

10 Wang, Y. *et al.* Structural and functional insights into 5'-ppp RNA pattern recognition by the innate immune receptor RIG-I. *Nat Struct Mol Biol* **17**, 781-787 (2010). https://doi.org:10.1038/nsmb.1863

11 Lu, C., Ranjith-Kumar, C. T., Hao, L., Kao, C. C. & Li, P. Crystal structure of RIG-I C-terminal domain bound to blunt-ended double-strand RNA without 5' triphosphate. *Nucleic Acids Res* **39**, 1565-1575 (2011). https://doi.org:10.1093/nar/gkq974

12 Lu, C. *et al.* The structural basis of 5' triphosphate double-stranded RNA recognition by RIG-I C-terminal domain. *Structure* **18**, 1032-1043 (2010). https://doi.org:10.1016/j.str.2010.05.007

13 Luo, D. *et al.* Structural insights into RNA recognition by RIG-I. *Cell* **147**, 409-422 (2011). https://doi.org:10.1016/j.cell.2011.09.023

316 14 Peisley, A., Wu, B., Yao, H., Walz, T. & Hur, S. RIG-I forms signaling-competent filaments
317 in an ATP-dependent, ubiquitin-independent manner. *Mol Cell* **51**, 573-583 (2013).
318 https://doi.org:10.1016/j.molcel.2013.07.024
319 15 Ramanathan, A. *et al.* The autoinhibitory CARD2-Hel2i Interface of RIG-I governs RNA
320 selection. *Nucleic Acids Res* **44**, 896-909 (2016). https://doi.org:10.1093/nar/gkv1299
321 16 Kim, D. H. *et al.* Interferon induction by siRNAs and ssRNAs synthesized by phage
322 polymerase. *Nat Biotechnol* **22**, 321-325 (2004). https://doi.org:10.1038/nbt940
323 17 Pichlmair, A. *et al.* RIG-I-mediated antiviral responses to single-stranded RNA bearing 5'-
324 phosphates. *Science* **314**, 997-1001 (2006). https://doi.org:10.1126/science.1132998
325 18 Schlee, M. *et al.* Recognition of 5' triphosphate by RIG-I helicase requires short blunt
326 double-stranded RNA as contained in panhandle of negative-strand virus. *Immunity* **31**,
327 25-34 (2009). https://doi.org:10.1016/j.immuni.2009.05.008
328 19 Schmidt, A. *et al.* 5'-triphosphate RNA requires base-paired structures to activate antiviral
329 signaling via RIG-I. *Proc Natl Acad Sci U S A* **106**, 12067-12072 (2009).
330 https://doi.org:10.1073/pnas.0900971106
331 20 Devarkar, S. C. *et al.* Structural basis for m7G recognition and 2'-O-methyl discrimination
332 in capped RNAs by the innate immune receptor RIG-I. *Proc Natl Acad Sci U S A* **113**, 596-
333 601 (2016). https://doi.org:10.1073/pnas.1515152113
334 21 Schuberth-Wagner, C. *et al.* A Conserved Histidine in the RNA Sensor RIG-I Controls
335 Immune Tolerance to N1-2'O-Methylated Self RNA. *Immunity* **43**, 41-51 (2015).
336 https://doi.org:10.1016/j.immuni.2015.06.015
337 22 Marques, J. T. *et al.* A structural basis for discriminating between self and nonself double-
338 stranded RNAs in mammalian cells. *Nat Biotechnol* **24**, 559-565 (2006).
339 https://doi.org:10.1038/nbt1205
340 23 Kato, H. *et al.* Length-dependent recognition of double-stranded ribonucleic acids by
341 retinoic acid-inducible gene-I and melanoma differentiation-associated gene 5. *J Exp Med*
342 **205**, 1601-1610 (2008). https://doi.org:10.1084/jem.20080091
343 24 Kato, H. *et al.* Differential roles of MDA5 and RIG-I helicases in the recognition of RNA
344 viruses. *Nature* **441**, 101-105 (2006). https://doi.org:10.1038/nature04734
345 25 Binder, M. *et al.* Molecular mechanism of signal perception and integration by the innate
346 immune sensor retinoic acid-inducible gene-I (RIG-I). *J Biol Chem* **286**, 27278-27287
347 (2011). https://doi.org:10.1074/jbc.M111.256974
348 26 Kohlway, A., Luo, D., Rawling, D. C., Ding, S. C. & Pyle, A. M. Defining the functional
349 determinants for RNA surveillance by RIG-I. *EMBO Rep* **14**, 772-779 (2013).
350 https://doi.org:10.1038/embor.2013.108
351 27 Linehan, M. M. *et al.* A minimal RNA ligand for potent RIG-I activation in living mice. *Sci*
352 *Adv* **4**, e1701854 (2018). https://doi.org:10.1126/sciadv.1701854
353 28 Baum, A., Sachidanandam, R. & García-Sastre, A. Preference of RIG-I for short viral RNA
354 molecules in infected cells revealed by next-generation sequencing. *Proc Natl Acad Sci U*
355 *S A* **107**, 16303-16308 (2010). https://doi.org:10.1073/pnas.1005077107
356 29 Mercado-López, X. *et al.* Highly immunostimulatory RNA derived from a Sendai virus
357 defective viral genome. *Vaccine* **31**, 5713-5721 (2013).
358 https://doi.org:10.1016/j.vaccine.2013.09.040

30 Sun, Y. *et al.* Immunostimulatory Defective Viral Genomes from Respiratory Syncytial Virus Promote a Strong Innate Antiviral Response during Infection in Mice and Humans. *PLoS Pathog* **11**, e1005122 (2015). https://doi.org:10.1371/journal.ppat.1005122

31 Kolakofsky, D. Isolation and characterization of Sendai virus DI-RNAs. *Cell* **8**, 547-555 (1976). https://doi.org:10.1016/0092-8674(76)90223-3

32 Lazzarini, R. A., Keene, J. D. & Schubert, M. The origins of defective interfering particles of the negative-strand RNA viruses. *Cell* **26**, 145-154 (1981). https://doi.org:10.1016/0092-8674(81)90298-1

33 Xu, J. *et al.* Identification of a Natural Viral RNA Motif That Optimizes Sensing of Viral RNA by RIG-I. *mBio* **6**, e01265-01215 (2015). https://doi.org:10.1128/mBio.01265-15

34 Sun, Y. *et al.* A specific sequence in the genome of respiratory syncytial virus regulates the generation of copy-back defective viral genomes. *PLoS Pathog* **15**, e1007707 (2019). https://doi.org:10.1371/journal.ppat.1007707

35 Welch, S. R. *et al.* Inhibition of Nipah Virus by Defective Interfering Particles. *J Infect Dis* **221**, S460-s470 (2020). https://doi.org:10.1093/infdis/jiz564

36 Stone, A. E. *et al.* Hepatitis C virus pathogen associated molecular pattern (PAMP) triggers production of lambda-interferons by human plasmacytoid dendritic cells. *PLoS Pathog* **9**, e1003316 (2013). https://doi.org:10.1371/journal.ppat.1003316

37 Zuker, M. & Stiegler, P. Optimal computer folding of large RNA sequences using thermodynamics and auxiliary information. *Nucleic Acids Res* **9**, 133-148 (1981). https://doi.org:10.1093/nar/9.1.133

38 Fisher, D. G., Gnazzo, V., Holthausen, D. J. & López, C. B. Non-standard viral genome-derived RNA activates TLR3 and type I IFN signaling to induce cDC1-dependent CD8+ T-cell responses during vaccination in mice. *Vaccine* **40**, 7270-7279 (2022). https://doi.org:10.1016/j.vaccine.2022.10.052

39 Gnazzo, V. *et al.* DDO-adjuvanted influenza A virus nucleoprotein mRNA vaccine induces robust humoral and cellular type 1 immune responses and protects mice from challenge. *mBio*, e0358924 (2024). https://doi.org:10.1128/mbio.03589-24

40 Fisher, D. G., Coppock, G. M. & López, C. B. Virus-derived immunostimulatory RNA induces type I IFN-dependent antibodies and T-cell responses during vaccination. *Vaccine* **36**, 4039-4045 (2018). https://doi.org:10.1016/j.vaccine.2018.05.100

41 Rehwinkel, J. & Gack, M. U. RIG-I-like receptors: their regulation and roles in RNA sensing. *Nat Rev Immunol* **20**, 537-551 (2020). https://doi.org:10.1038/s41577-020-0288-3

42 Gokhale, N. S. *et al.* Cellular RNA interacts with MAVS to promote antiviral signaling. *Science* **386**, eadl0429 (2024). https://doi.org:10.1126/science.adl0429

43 Boulias, K. & Greer, E. L. Biological roles of adenine methylation in RNA. *Nat Rev Genet* **24**, 143-160 (2023). https://doi.org:10.1038/s41576-022-00534-0

44 Jiang, X. *et al.* Intratumoral delivery of RIG-I agonist SLR14 induces robust antitumor responses. *J Exp Med* **216**, 2854-2868 (2019). https://doi.org:10.1084/jem.20190801

45 Mao, T. *et al.* A stem-loop RNA RIG-I agonist protects against acute and chronic SARS-CoV-2 infection in mice. *J Exp Med* **219** (2022). https://doi.org:10.1084/jem.20211818

402 **FIGURE LEGENDS**

**Figure 1. CbVG IFN Activation**

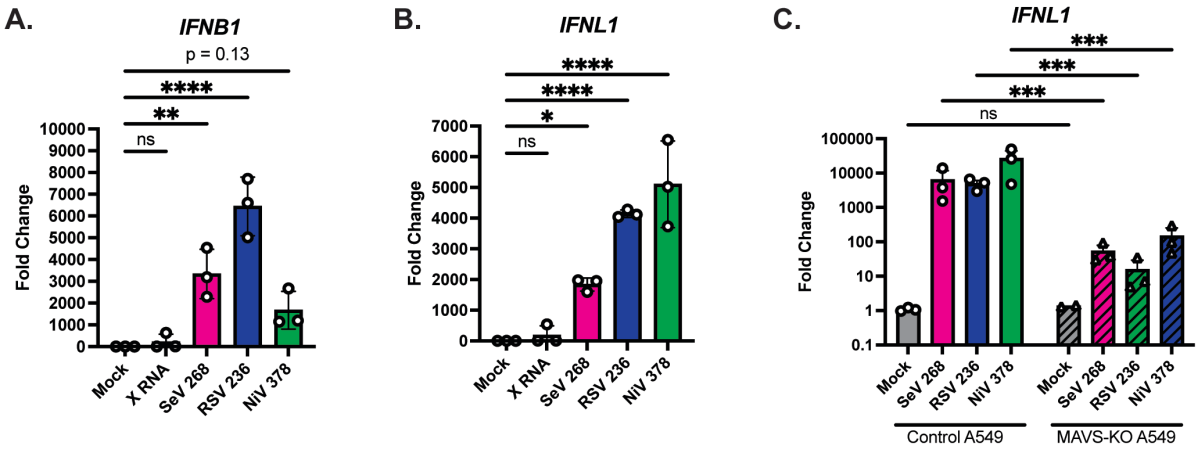


403

404 **Figure 1. CbVG from RSV and NiV induce MAVS-dependent IFN expression. (A+B)**
405 Quantitative PCR (qPCR) for (A) type I interferon (*IFNB1*) and (B) type III interferon
406 (*IFNL1*) expression by A549 cells at 6 hours post transfection (hpt) with 5 pmol of HCV X
407 RNA, SeV cbVG 268, RSV cbVG 236, or NiV cbVG 378. One-way ANOVA was performed
408 for statistical analysis. ns: $p>0.05$; *: $p<0.05$, ***: $p<0.001$; ****: $p<0.0001$. Data are
409 represented as fold change over Mock. (C) qPCR for *IFNL1* of control or MAVS-KO A549
410 cells at 6 hpt with 5 pmol of SeV cbVG 268, RSV cbVG 236, or NiV cbVG 378. One-way
411 ANOVA was performed for statistical analysis. ****: $p<0.0001$. Data are represented as
412 fold change over Mock. Data reported are biological triplicates.

413

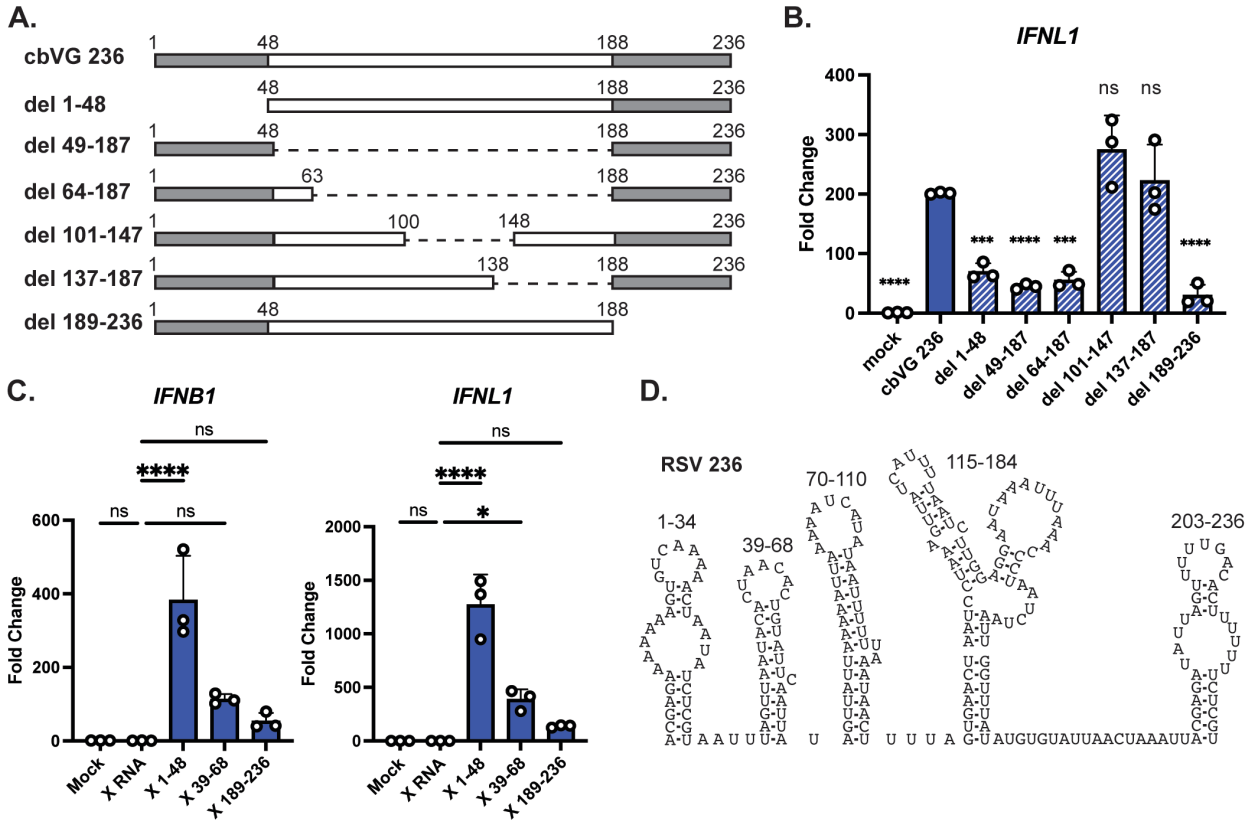


**Figure 2. RSV cbVG sequences 1-48 and 39-68 are immunostimulatory.** (A) Indicated deletions of RSV cbVG 236 were generated by *in vitro* transcription then 1 pmol of IVT RNA was transfected into A549 cells. (B) Expression of *IFNL1* was measured by qPCR at 6 hpt. One-way ANOVA was performed for statistical analysis. ns: $p>0.05$; ***: $p<0.001$, ****: $p<0.0001$. Data are represented as fold change over cbVG 236. (C) Sequences from RSV cbVG 236 were attached to X RNA then *in vitro* transcribed. 1 pmol of RNA was transfected into A549 cells and expression of *IFNB1* and *IFNL1* was measured by qPCR at 6 hpt. One-way ANOVA was performed for statistical analysis. ns: $p>0.05$; *: $p<0.05$, ****: $p<0.0001$. Data are represented as fold change over the X RNA control. (D) Predicted structure of RNA stem loops from RSV cbVG 236. Data reported are biological triplicates.

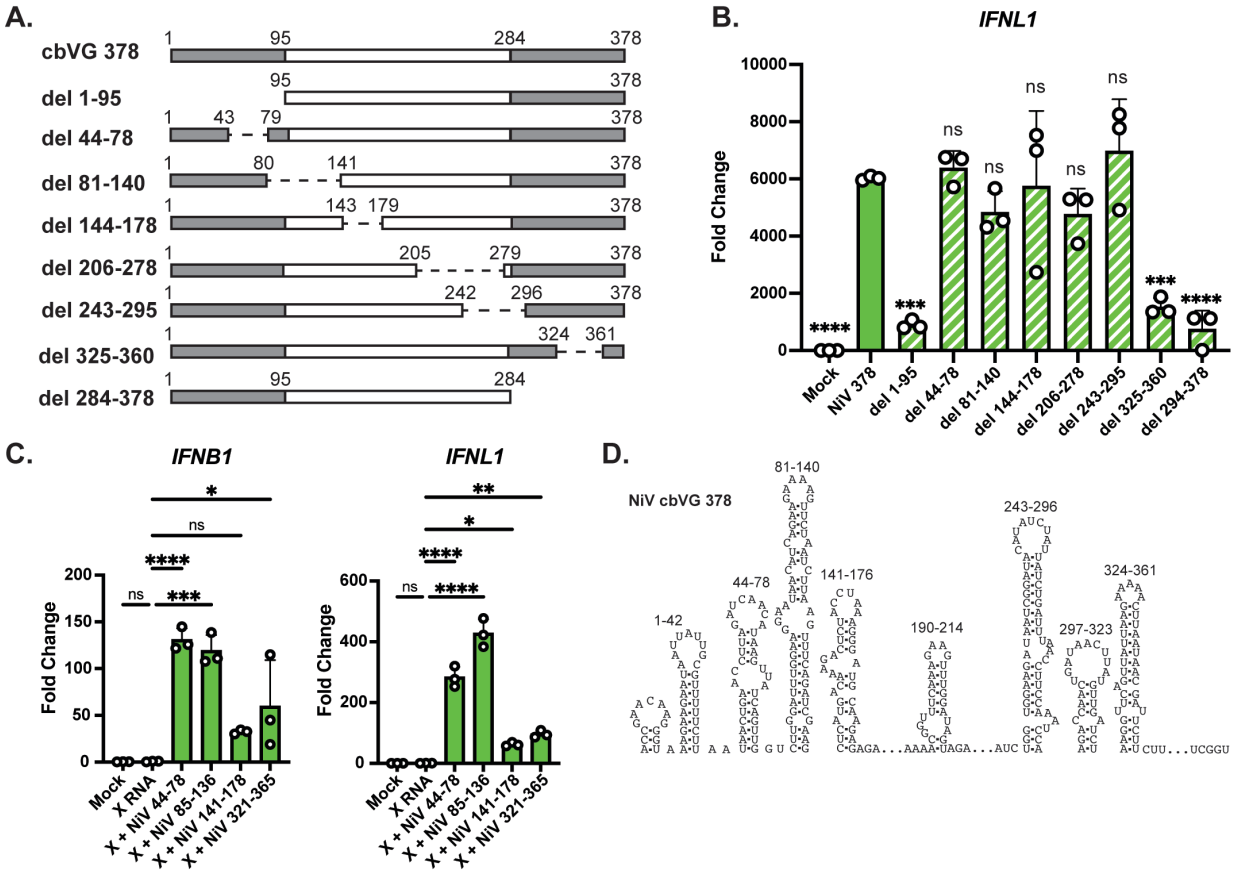


**Figure 3. NiV cbVG sequences 44-78 and 85-136 are immunostimulatory.** (A) Indicated deletions of NiV cbVG 378 were generated by *in vitro* transcription then 1 pmol of IVT RNA was transfected into A549 cells. (B) Expression of *IFNL1* was measured by qPCR at 6 hpt. One-way ANOVA was performed for statistical analysis. ns: p>0.05; ***: p<0.001, ****: p<0.0001. Data are represented as fold change over cbVG 378. (C) Sequences from NiV cbVG 378 were attached to X RNA then *in vitro* transcribed. 1 pmol of IVT RNA was transfected into A549 cells and expression of *IFNB1* and *IFNL1* was measured by qPCR at 6 hpt.. One-way ANOVA was performed for statistical analysis. ns: p>0.05; *: p<0.05, **: p<0.01; ***: P<0.001; ****: p<0.0001. Data are represented as fold change over the X RNA control. (D) Predicted structure of RNA stem loops from NiV cbVG 378. Data reported are biological triplicates.

439

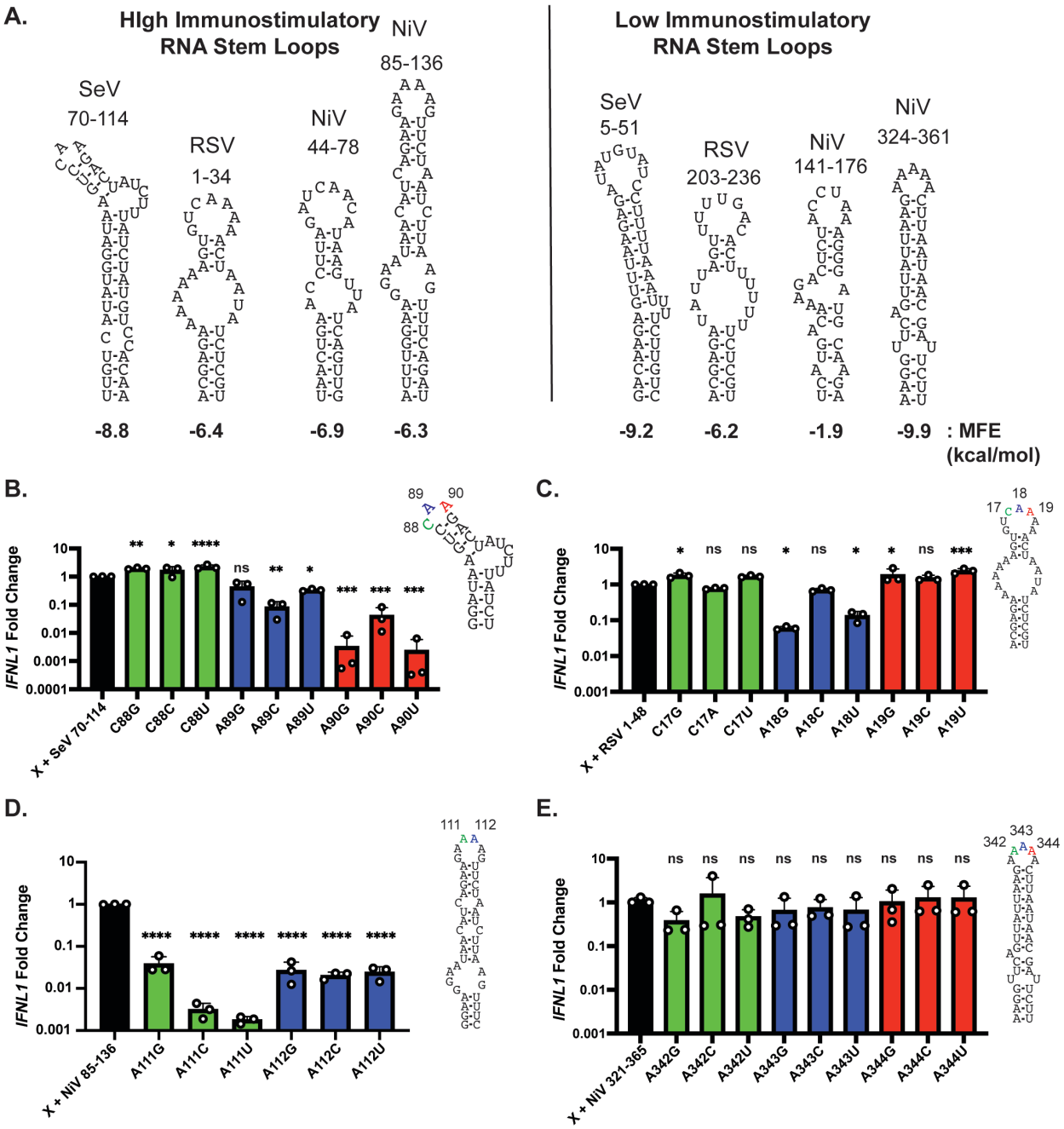


440

441 **Figure 4. Terminal loop adenines are necessary for high IFN expression.** (A)
442 Predicted RNA structures of high immunostimulatory and low immunostimulatory stem
443 loops derived from cbVGs. (B-E) Indicated mutations were generated for cbVG
444 sequences attached to the X RNA. The following sequences were mutated: (B) SeV 70-

114, (C) RSV 1-48, (D) NiV 85-136, and (E) NiV 324-361. RNAs were *in vitro* transcribed and 1 pmol of IVT RNA was transfected into A549 cells. Expression of *IFNL1* was measured by qPCR at 6 hpt. One-way ANOVAs were performed for statistical analysis. ns: p>0.05; *: p<0.05, **: p<0.01; ***: P<0.001; ****: p<0.0001. Data are represented as fold change over the wild-type stem loops. Data reported are biological triplicates.

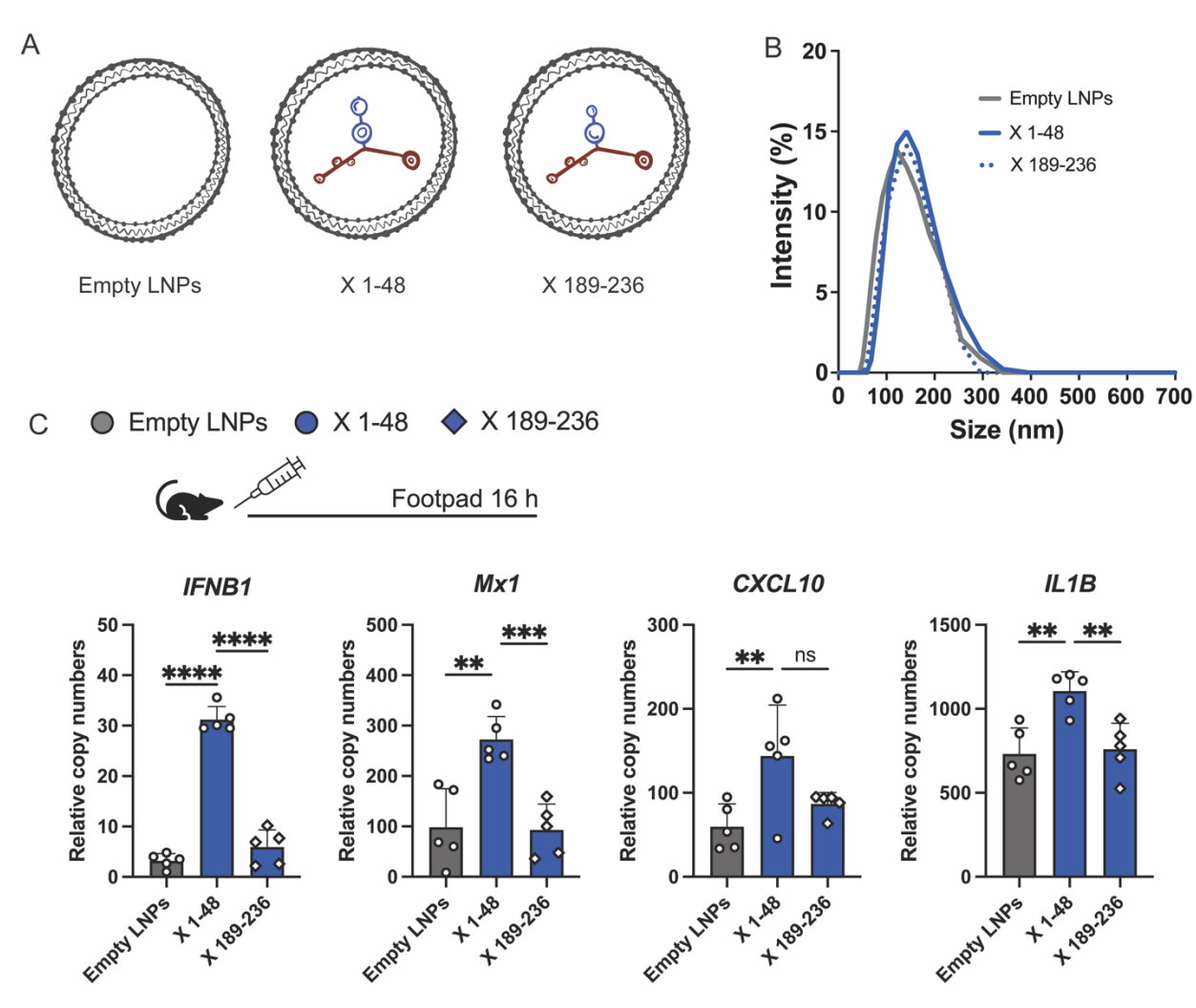


**Figure 5. X + RSV 1-48 activates innate immune signaling in mice. (**A) Schematic of lipid nanoparticles (LNPs) containing X + RSV 1-48 (X 1-48) or X + RSV 189-236 (X 189-236). (B) Dynamic light scattering measurement of LNP sizes of empty LNPs, X 1-48, and

455 X 189-236. (C) LNPs were injected subcutaneously into the footpad of mice. Sixteen
456 hours post injection, RNA was collected and the RNA expression of *IFNB1*, *MX1*,
457 *CXCL10*, and *IL1B* was quantified by qPCR. One-way ANOVAs were performed for
458 statistical analysis. ns: $p>0.05$; **: $p<0.01$; ***: $P<0.001$; ****: $p<0.0001$. Data reported are
459 5 individual mice.